Geophysical Research Letters

RESEARCH LETTER
10.1029/2023GL104191

Key Points:

- The sea-level variance explained by regional forcings increases with time north of Cape Hatteras due to the Inverted Barometer effect
- Lower sea level pressure centered around Mid-Atlantic Bight favors more contributions of the Inverted Barometer effect in recent decades
- The summertime North Atlantic Oscillation is largely responsible for the increased role of the Inverted Barometer effect

Supporting Information:

Supporting Information may be found in the online version of this article.

Correspondence to:

Y. Zhu,
Yingli.Zhu@colorado.edu

Citation:

Zhu, Y., Han, W., & Alexander, M. A. (2023). Nonstationary roles of regional forcings in driving low-frequency sea level variability along the U.S. east coast since the 1950s. *Geophysical Research Letters*, *50*, e2023GL104191. https://doi.org/10.1029/2023GL104191

Received 18 APR 2023
Accepted 18 JUL 2023

Nonstationary Roles of Regional Forcings in Driving Low-Frequency Sea Level Variability Along the U.S. East Coast Since the 1950s

Yingli Zhu[1], Weiqing Han[1], and Michael A. Alexander[2]

[1]Department of Atmospheric and Oceanic Sciences, University of Colorado, Boulder, CO, USA, [2]Physical Science Division, NOAA/Earth System Research Laboratory, Boulder, CO, USA

Abstract The nonstationary roles of regional forcings from alongshore wind stress and sea level pressure (SLP) in driving low-frequency (interannual-to-decadal) sea level variability along the U.S. east coast for the 1959–2020 period are investigated. The role of regional forcings increases with time north of Cape Hatteras particularly during summer when their contributions to the variance of observed summertime coastal sea level anomalies increase by approximately 58%–87% from 1959–1989 to 1990–2020. The enhanced impact of regional forcings in recent decades results from an increase in the Inverted Barometer (IB) effect that act constructively with alongshore wind stress especially during summer, and to a lesser extent for the Gulf of Maine during fall. The summertime North Atlantic Oscillation (NAO) is largely responsible for the increased IB effect, owing to the stronger NAO-associated low SLP anomalies centered around the Mid-Atlantic Bight in recent decades compared to earlier decades.

Plain Language Summary Alongshore wind stress and sea level pressure (SLP) are important regional forces in driving low-frequency (interannual-to-decadal) sea level anomalies along the U.S. east coast. The roles of these regional forcings, however, vary with time, season, and region, which can shift the location and change the frequency and intensity of coastal flooding. In this study, we find that regional forcings contribute more to observed sea level variability north of Cape Hatteras in recent decades (1990–2020) compared to earlier decades (1959–1989), particularly during summer. The increased role of regional forcings results from SLP variability via the Inverted Barometer (IB) effect, which exhibits a significant upward trend during summer with lower (higher) SLP raising (suppressing) sea level. The North Atlantic Oscillation (NAO) is largely responsible for the increased role of IB effect because the lower SLP anomalies related to the NAO have become more prominent north of Cape Hatteras in recent decades. Although winter NAO has been shown to be important for affecting the coastal sea level anomalies, it is the summer NAO effect that is enhanced via the IB effect, accounting for the enhanced regional forcing in recent decades.

1. Introduction

Sea level variability influences coastal flooding and erosion along the global coasts, including the U.S. east coast (USEC; e.g., Cazenave & Le Cozannet, 2014; Neumann et al., 2015; Wdowinski et al., 2016). In particular, low-frequency (interannual to decadal) sea level anomalies (SLAs) have large fluctuations, which can shift the location and change the frequency and intensity of coastal flooding along the USEC (e.g., Li et al., 2022; Sweet et al., 2019, 2021).

The physical drivers of USEC interannual to decadal SLAs include both local forcing over the shelf and remote forcing from the open ocean (e.g., reviews of Han et al., 2019; Hughes et al., 2019; Piecuch et al., 2019; Ponte et al., 2019; Woodworth et al., 2019). Previous studies have demonstrated the importance of regional forcings, including alongshore wind stress over the shelf, local sea level pressure (SLP) through the Inverted Barometer (IB) effect, and river discharges in causing interannual to decadal SLAs along the USEC, especially north of Cape Hatteras (e.g., Blaha, 1984; Li et al., 2014; Piecuch, Dangendorf, et al., 2016; Piecuch, Thompson, & Donohue, 2016; Piecuch et al., 2018; Piecuch & Ponte, 2015; Woodworth et al., 2014). Remote forcing from the open ocean to the east, and coastal wave propagation and advection from the subpolar region to the north can also influence USEC sea level (e.g., Bingham & Hughes, 2009; Diabaté et al., 2021; Ezer, 2013; Ezer, 2019; Ezer et al., 2013; Frederikse et al., 2017; Frederikse et al., 2022; Hong et al., 2000; Little et al., 2017; Minobe et al., 2017; Thompson & Mitchum, 2014; Wang et al., 2022; Yin & Goddard, 2013). We focus on regional

forcings starting from the 1950s when much more tide gauge measurements and more accurate regional SLP and wind stress data are available (e.g., Bell et al., 2021).

The USEC SLAs and their regional drivers, however, are nonstationary and they vary with time, location, and variability period (e.g., Little et al., 2021). For instance, accelerated sea level rise (SLR) was detected north of Cape Hatteras for 1950–2009 (Sallenger et al., 2012), while decelerated SLR north of Cape Hatteras was seen from 2010 to 2015 and the SLR acceleration shifted to the south of Cape Hatteras during this time (Domingues et al., 2018; Valle-Levinson et al., 2017). As the dominant regional forcing, the nearshore wind especially the alongshore wind stress alters the coastal SLAs via Ekman transport convergence/divergence and plays a larger role north of Cape Hatteras than south of Cape Hatteras (Andres et al., 2013; Blaha, 1984; Hong et al., 2000; Piecuch, Dangendorf, et al., 2016; Piecuch, Thompson, & Donohue, 2016; Woodworth et al., 2014). It has also been shown that the IB effect varies with the analysis time period (Piecuch & Ponte, 2015).

The regional wind and SLP that affect coastal SLAs are related to climate variability modes, particularly the North Atlantic Oscillation (NAO), the Atlantic Multidecadal Oscillation (AMO) and the El Niño–Southern Oscillation (ENSO) (Goddard et al., 2015; Hamlington et al., 2015; Han et al., 2019; Park & Dusek, 2013; Sweet & Zervas, 2011). Moreover, the impact of climate modes on coastal SLAs exhibits interdecadal variability. For instance, the NAO's relationship to interannual SLAs along the USEC north of Cape Hatteras is weak before ∼1987 but strong after ∼1987 (Andres et al., 2013; Kenigson et al., 2018), due to the regional shift of the NAO action center and the associated surface wind patterns (Kenigson et al., 2018). These studies, however, used annual mean records to assess the SLAs and their relationships with climate modes without considering the seasonality of low-frequency sea level variability (e.g., Andres et al., 2013; Kenigson et al., 2018; Piecuch & Ponte, 2015). The important science issues to be addressed here are: How does the nonstationary impact of regional forcings of coastal SLAs vary with season and region? How are the time-varying regional forcings linked to variations of atmospheric circulation patterns, and how do the NAO, AMO and ENSO influence the atmospheric circulation patterns and contribute to the nonstationary roles of regional forcings in causing the observed coastal SLAs?

In this study, we focus on addressing these issues through observational analysis and application of simplified dynamic models as well as a Bayesian Dynamic Linear Model (DLM). The rest of the paper is organized as follows. In Section 2, we describe the data sets and methods used in this study. In Section 3, we examine the nonstationary roles of regional forcings in driving the low-frequency coastal SLAs along the USEC in different seasons and regions and explore the associated changes of atmospheric circulation patterns. In Section 4, we explore the effects of climate modes on the nonstationary impact of regional forcings in driving USEC SLAs. In Section 5 we summarize our results and discuss their implications.

2. Data and Methods

2.1. Data

Tide-gauge observed monthly mean sea level data from the Permanent Service for Mean Sea Level (PSMSL, 2021; Holgate et al., 2013) are used to analyze the low-frequency SLAs along the USEC. Tide gauges located in bays and estuaries are excluded. We select the tide gauges with data available for more than 70% of the time during the 1959–2020 period when more tide-gauge observed sea level are available than the earlier 20th century (Figure 1a and Table S1 in Supporting Information S1). We spatially average the observed SLAs in three regions: the South Atlantic Bight (SAB), Mid-Atlantic Bight (MAB) and Gulf of Maine (GOM) (Figure 1a), because interannual-to-decadal coastal SLAs are generally coherent within each region but differ between regions (e.g., Little et al., 2021; Woodworth et al., 2014).

The monthly surface wind stress and SLP from the European Centre for Medium-Range Weather Forecasts reanalysis v5 (ERA5; Hersbach et al., 2019) are used to estimate coastal SLAs induced by alongshore wind stress and the IB effect, respectively. The ERA5 quality has improved steadily since 1950s (Bell et al., 2021). The NAO, AMO and ENSO indices from 1959 to 2020 (see Text S1 in Supporting Information S1 for definitions) are used to examine the effects of the NAO, AMO and ENSO on regional forcings (i.e., surface wind and SLP) and on coastal SLAs. Note that the monthly mean climatology and linear trend of each variable for the 1959–2020 period are removed to obtain their anomalies. Therefore, the monthly anomalies analyzed in this paper primarily represent low-frequency variability at interannual-to-decadal timescales.

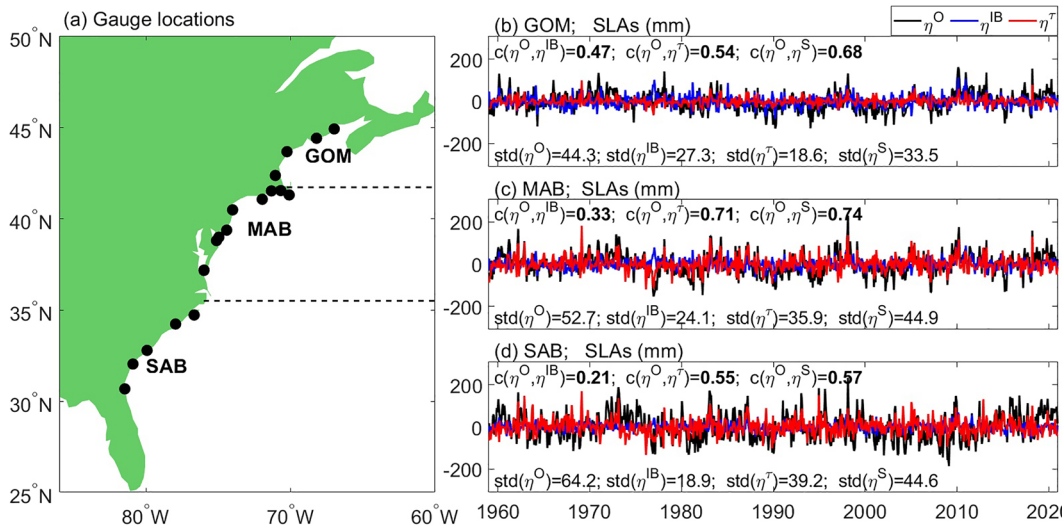

Figure 1. (a) Locations of tide gauges (black dots). Zonal dashed lines separate gauges located in the SAB, MAB and GOM. (b–d) Regional mean monthly SLAs observed by tide gauges (η^{O}) and due to the IB effect (η^{IB}), alongshore wind stress (η^{τ}) and their sum (η^{S}) in the GOM, MAB and SAB, respectively. The monthly climatology and linear trend of each variable are removed. Correlations between observed and estimated SLAs driven by regional forcings are shown in the upper part of (b)–(d) and statistically significant correlations (≥95% confidence) are in bold. Standard deviations (std; mm) of observed and estimated SLAs driven by regional forcings are shown in the lower part of (b)–(d).

2.2. The Bayesian Dynamic Linear Model

The Bayesian DLM allows for temporal variability in the regression coefficients, as opposed to fixed coefficients used in standard linear regression models (Petris et al., 2009). Therefore, the DLM is used to examine the temporally nonstationary relationship between the regionally driven coastal SLAs and climate modes. The Bayesian DLM consists of an observation Equation 1 and a state Equation 2:

$$y(t) = b_0(t) + b_1(t)x_1(t) + \ldots + b_M(t)x_M(t) + \epsilon(t), \quad \epsilon(t) \sim N(0, V), \tag{1}$$

$$b_i(t) = b_i(t-1) + w_i(t), \quad w_i(t) \sim N(0, W_i), \tag{2}$$

where y is observation and is predicted by M independent predictors x_i (x_1,…x_M), b_i ($i = 0, 1, 2,\ldots,M$) are coefficients that evolve in time based on the state Equation 2 which measures the dynamical impacts of x_i on y, ϵ and w are errors distributed normally with a mean of zero and variances of $V(t)$ and $W_i(t)$ and N represents normal distribution. Using the NAO index as predictor in the DLM (Section 4) results in residuals (i.e., errors) that have an approximately normal distribution and small autocorrelations (Figure S1 in Supporting Information S1). Regression coefficients b_i are obtained by applying Kalman filtering and smoothing. Variances $V(t)$ and $W_i(t)$ are obtained using the maximum likelihood estimation method (Petris et al., 2009). More details of DLM are described in previous studies (e.g., Han et al., 2017; Han et al., 2018; Laine et al., 2014; Petris et al., 2009). In Equation 1, y represents coastal SLA induced by regional forcings, primarily by SLP and wind stress anomalies, and x_i are the predictors representing the NAO, AMO and ENSO indices. In addition to SLP and wind stress, we have also examined the effect of river discharges, another regional forcing that can affect coastal SLA, but their influence is negligible (Figure S2 in Supporting Information S1) and thus is not discussed further.

3. Effects of Regional Forcings and Their Nonstationary Impacts

3.1. Effects of Regional Forcings and Seasonality

We apply simplified dynamical models (described in Text S2 in Supporting Information S1) to estimate the regionally forced coastal SLAs due to alongshore wind stress (η^{τ}) and the IB effect (η^{IB}) in the SAB, MAB and GOM from 1959 to 2020. The coastal SLAs induced by alongshore wind stress have higher correlations with the observations than IB effect in all three regions (Figures 1b–1d). While the alongshore wind stress forcing is more influential than the IB effect in the SAB and MAB for the entire period of 1959–2020, the SLA magnitudes,

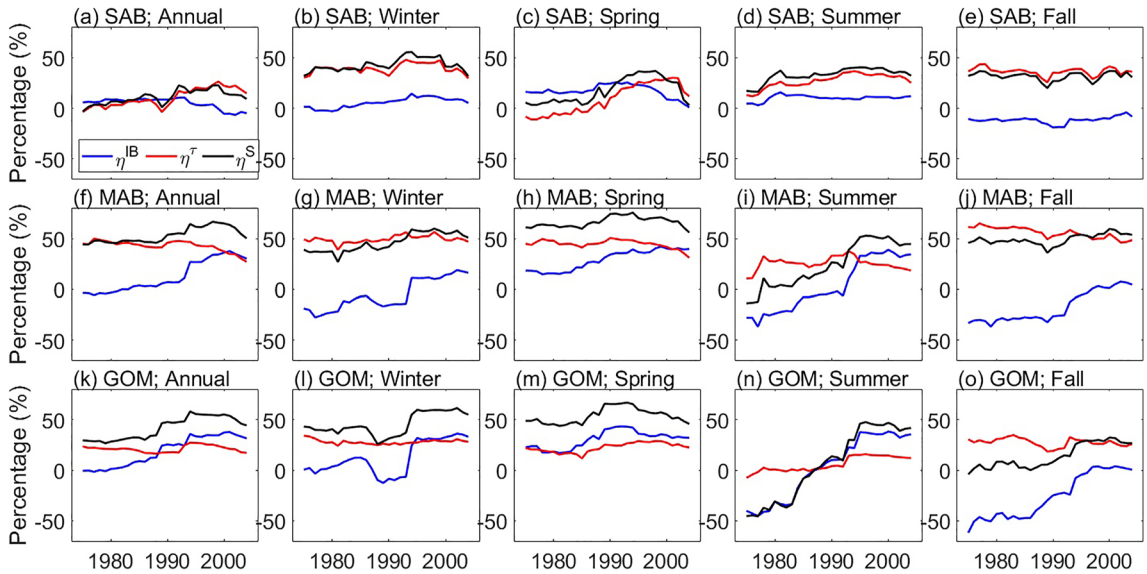

Figure 2. The 31-year moving percentage of tide gauge observed sea level variance explained by the alongshore wind stress (η^{τ}), the IB effect (η^{IB}), and their sum ($\eta^{S} = \eta^{IB} + \eta^{\tau}$) for annual mean and each season in (a–e) the SAB, (f–j) the MAB and (k–o) the GOM. The time in the *x*-axis is the middle point in each 31-year moving window. The percentage of variance explained by regional forcings is defined as $\left[1 - \frac{\mathrm{var}(\eta^{OBS} - \eta^{EST})}{\mathrm{var}(\eta^{OBS})}\right] \times 100\%$ (e.g., Piecuch & Ponte, 2015), where var represents computing variance, and η^{OBS} represents tide-gauge observed SLAs and η^{EST} is η^{IB}, η^{τ} and η^{S}, respectively.

measured by SLA standard deviation, due to the IB effect are larger than that due to alongshore wind stress in the GOM. The magnitudes of total regionally forced SLAs, $\eta^{S} = \eta^{IB} + \eta^{\tau}$, are smaller than observed in all three regions, suggesting that other forcings can also play a significant role, as discussed in Section 1.

The impacts of regional forcings on low-frequency USEC SLAs vary with season, with the largest variability occurring in winter (December-February) in all three regions and the smallest in summer (June-August) (Figure S3 in Supporting Information S1). The standard deviations of the regionally forced SLAs and their correlations with tide gauge observations show that in the SAB and MAB, alongshore wind stress has a larger impact than the IB effect throughout the year except for summer in MAB. By contrast, in the GOM the IB-induced SLAs are consistently larger than that due to the alongshore wind in all seasons (Figure S3 in Supporting Information S1). Ponte (2006) also found that the IB effect becomes larger at higher latitudes.

3.2. Nonstationary Roles of Regional Forcings

We next examine the nonstationary roles of regional forcings for each season. Using a 31-year moving window, which allows for a direct comparison between the first and second half of the 62-year study period, we calculate the correlations between the regionally forced and observed SLAs (Figure S4 in Supporting Information S1) and the percentages of observed sea level variance explained by regional forcings in each season (Figure 2). We have also tested 20-year and 40-year moving windows, and the results do not change qualitatively (not shown).

In the SAB, the observed variance explained by regionally forced total SLAs are relatively stable over the study period for all seasons (Figures 2a–2e, black lines). By contrast, in the GOM and to a lesser extent the MAB, annual mean total regional forcings explain more of the observed variance during recent decades compared to earlier decades (Figures 2f and 2k, black lines), with statistically significant linear trends of 0.69 ± 0.53%/year (±2σ) and 1.09 ± 0.70%/year (±2σ) in the MAB and GOM, respectively. The uncertainty in the linear trend, 2σ, is given as two times standard trend error with an effective degree of freedom $N^{*} = \frac{1-r}{1+r}$, where r is the first-order autoregressive coefficient obtained from the trend residual. The increased variance explained by total regional forcings results from the increased variance explained by the IB effect, with linear trends of 1.66 ± 0.67%/year (±2σ) and 1.60 ± 0.43%/year (±2σ) in the MAB and GOM, respectively (Figures 2f and 2k). While the original time series have been detrended, trends can occur in Figure 2 due to a change in the relationship between the forcings and SLAs.

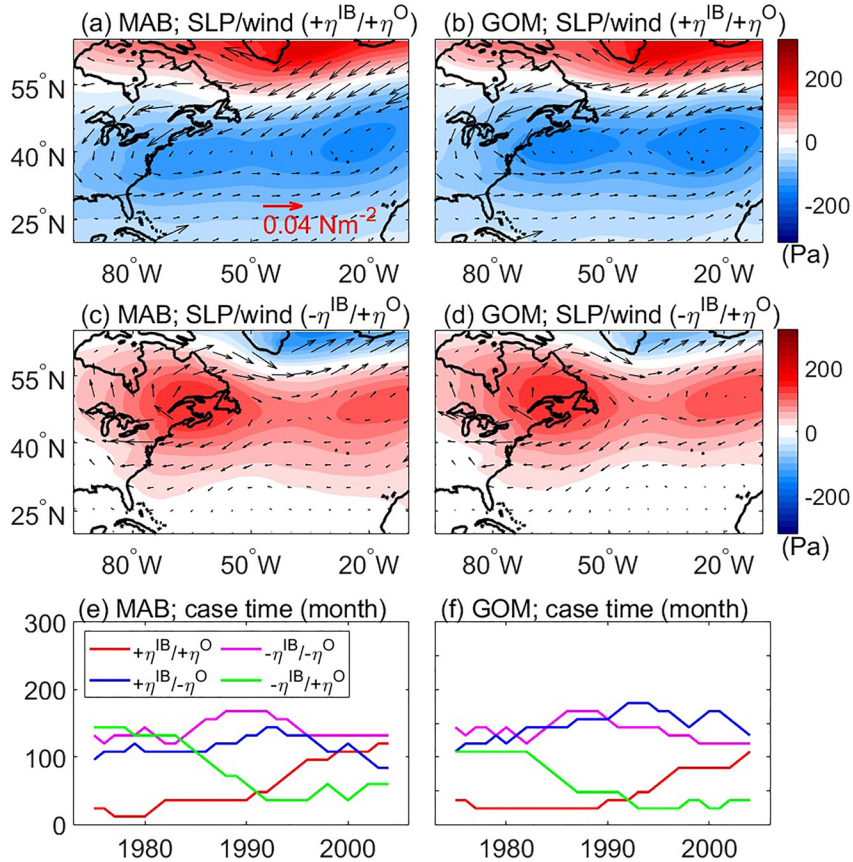

Figure 3. (a–b) Composite maps of sea level pressure (SLP; Pa) and wind stress (Nm^{-2}) anomalies for the east U.S. and northwestern Atlantic Ocean during summer, when IB-induced coastal SLAs in the MAB and GOM and observed coastal SLAs are both positive, $+\eta^{IB}/+\eta^{O}$. (c–d) Same as (a–b) but for negative IB-induced coastal SLAs and positive observations ($-\eta^{IB}/+\eta^{O}$). (e) The 31-year moving number of months when the IB-induced and observed coastal SLAs have same signs ($+\eta^{IB}/+\eta^{O}$; $-\eta^{IB}/-\eta^{O}$) and have opposite signs ($-\eta^{IB}/+\eta^{O}$; $+\eta^{IB}/-\eta^{O}$) in the MAB during summer. (f) Same as (e) but for the coastal SLAs in the GOM. The time in the *x*-axis of (e–f) is the middle point in each 31-year moving window.

The most noticeable increase in the effects of regional forcings occurs in summer, and results mainly from the increased IB effect (Figures 2i and 2n), with weaker but visible enhancement appearing in winter and fall (September–November) (Figure 2f–2o; Figures S5 and S6 in Supporting Information S1). In particular, the observed summertime sea level variance explained by the total regional forcings increases by 58.4% and 87.1% with statistically significant linear trends of 2.36 ± 0.67%/year and 3.80 ± 1.09%/year in the MAB and GOM, respectively. During the summer season of earlier decades (1959–1989), regional forcings have little or negative contributions to the observed SLAs in the MAB and GOM (Figures 2i and 2n), indicating that other forcings dominate the observed SLAs. During recent decades (1990–2020), the IB effect is the most important regional forcing in summer and significantly contributes to the observed coastal SLAs, with statistically significant linear trends of 2.78 ± 0.77%/year and 3.39 ± 0.99%/year in the MAB and GOM, respectively. Although previous studies have shown that regional forcings are not stationary (e.g., Piecuch et al., 2018; Piecuch & Ponte, 2015), we find that the largest nonstationarity occurs during summer at the USEC north of Cape Hatteras, due to the IB effect.

To understand why the IB effect increased dramatically in recent decades, we analyze the times when the IB effect enhances or reduces SLAs (Figures 3a–3d). When IB-induced coastal SLAs have the same sign as observed ($+\eta^{IB}/+\eta^{O}$ and $-\eta^{IB}/-\eta^{O}$), they increase the amplitude of the SLAs. For instance, when both the IB induced and observed SLAs are positive ($+\eta^{IB}/+\eta^{O}$), negative SLP anomalies occupy the entire USEC centered around the MAB (Figures 3a and 3b). Alongshore wind stress and SLP north of Cape Hatteras act constructively, with northeasterly wind anomalies increasing coastal sea level by inducing onshore Ekman transport, which enhances the high sea level caused by negative SLP anomalies via the IB effect. The reverse occurs when the IB forcing

and coastal SLAs have the opposite sign ($-\eta^{IB}/+\eta^{O}$ and $+\eta^{IB}/-\eta^{O}$). During periods when IB-induced coastal SLAs are negative and observed SLAs are positive ($-\eta^{IB}/+\eta^{O}$), positive SLP anomalies cover the USEC centered around the Gulf of St. Lawrence (Figures 3c and 3d). Alongshore wind stress and SLP north of Cape Hatteras act destructively, with northeasterly wind anomalies increasing coastal sea level, which compensates for the low sea level induced by positive SLP anomalies. In addition, when the atmospheric circulation center is located further south, SLP anomalies are strengthened in the USEC region and so is the IB effect (Figures 3a and 3b), compared to periods with a negative contribution (Figures 3c and 3d). The composite circulation patterns for $-\eta^{IB}/-\eta^{O}$ and $+\eta^{IB}/-\eta^{O}$ cases (Figure S7 in Supporting Information S1) are similar to those of $+\eta^{IB}/+\eta^{O}$ and $-\eta^{IB}/+\eta^{O}$, respectively, except for reversed signs of the SLP and wind stress anomalies.

We further count the number of months during summer season for each of the four categories during the 31-year moving window (Figures 3e and 3f) and find that the number of months with a positive contribution ($+\eta^{IB}/+\eta^{O}$) (Figures 3a and 3b) has an upward trend in the MAB and GOM (red lines of Figures 3e and 3f), while the negative contribution ($-\eta^{IB}/+\eta^{O}$) (Figures 3c and 3d) has a decreasing trend from 1959 to 2020 (green lines of Figures 3e and 3f). Similar trends also occur during fall (Figure S8 in Supporting Information S1). The cases for $-\eta^{IB}/-\eta^{O}$ and $+\eta^{IB}/-\eta^{O}$ have no apparent trends (blue and magenta lines of Figures 3e and 3f). These results suggest the anomalous wind and SLP patterns with the alongshore wind stress and SLP anomalies acting constructively during the recent decades (Figures 3a and 3b) whereas the alongshore wind stress and SLP anomalies acting destructively in the earlier decades (Figures 3c and 3d). Consistent with the increase in time with positive contributions ($+\eta^{IB}/+\eta^{O}$) and the decrease in time with negative contributions ($-\eta^{IB}/+\eta^{O}$), stronger negative SLP anomalies occur along the USEC during summer and fall in recent decades compared to the earlier decades (Figure S9 in Supporting Information S1).

4. Contribution of Climate Modes to Regionally Forced SLAs

To explore the effects of climate modes on atmospheric circulation variability and SLAs, we apply the Bayesian DLM with the predictand being the IB-induced coastal SLA and the predictor being the normalized indices of the NAO, AMO and ENSO. The product of DLM coefficient and predictor yields the coastal SLA induced by a climate mode (Equation 1 of Section 2.2). Our DLM results show that the AMO and ENSO have negligible influence on the IB-induced coastal SLAs throughout the analysis period (Figure S10 in Supporting Infromation S1). Therefore, we focus on the NAO. The NAO-related SLAs in the MAB and GOM for the summer season explain more observed sea level variance in recent decades compared to earlier decades (Figure 4a). Since the DLM coefficient is negative (Figure 4b), a negative NAO corresponds to positive IB-induced coastal SLA. The decadal shift of the NAO index from more positive values in earlier decades (1959–1989) to more negative values in recent decades (1990–2020; Figure 4c) indicates that the NAO tends to increase the number of $+\eta^{IB}/+\eta^{O}$ cases and reduce the number of $-\eta^{IB}/+\eta^{O}$ cases in recent decades, consistent with our analysis above (Figures 3e and 3f). Additionally, the larger DLM coefficient value in the MAB during recent decades (Figure 4b) indicates enhanced NAO influence on SLAs.

To understand why the NAO impact is enhanced, we compare SLP and wind stress anomalies due to the NAO between the earlier (1959–1989) and recent (1990–2020) periods during summer (Figures 4d–4f and 4g–4i). At each grid point, we apply the Bayesian DLM with normalized NAO index as the predictor and the SLP (or wind stress) anomaly as the predictand. The SLP (or wind stress) anomaly induced by the NAO is the product of the DLM coefficient and the NAO index. Figures 4d and 4e show composite maps of NAO-induced SLP and surface wind anomalies in the summers when observed SLAs in the MAB and GOM are positive, which resemble Figures 3c and 3d (3a and 3b) during earlier (recent) decades. During earlier decades, the IB-induced negative SLAs due to positive SLP in the MAB and GOM are associated with the positive NAO, having negative contribution to observed positive SLAs. During recent decades, the IB-induced positive SLAs due to negative SLP are associated with the negative NAO, having positive contribution to observed positive SLAs. The center of negative SLP anomaly in recent decades is shifted southward to the MAB compared to that of positive SLP anomaly during earlier decades (compare Figures 4d and 4e), causing an increased Bayesian DLM coefficient (Figure 4b) and making the NAO more effective in affecting MAB sea level.

While the composites shown in Figures 4d–4f include both interannual and decadal anomalies, Figures 4g–4i shows decadal anomalies averaged for 1959–1989 and 1990–2020 and their differences, demonstrating similar patterns with Figures 4d–4f except for weaker magnitudes. The decadal SLP anomalies are consistent with the

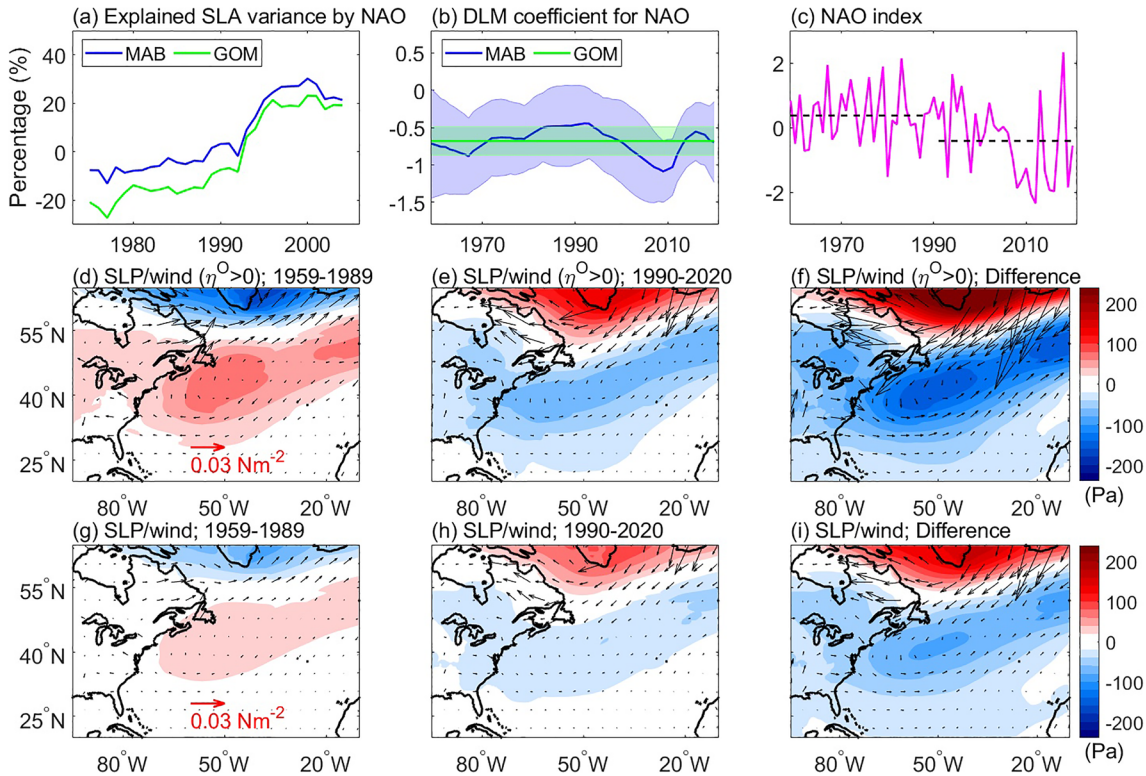

Figure 4. (a) The 31-year moving percentages of observed sea level variance explained by the NAO in the MAB and GOM during summer. The time in the *x*-axis is the middle point in each 31-year moving window. (b) Time-varying coefficients of Bayesian DLM for the NAO in the MAB and GOM. The shading represents ±2σ, where σ is the standard deviation of DLM coefficient. (c) The NAO index during summer. The averaged NAO index for the earlier (1959–1989) and recent (1990–2020) decades is shown in black dashed lines. (d) Composite SLP (Pa) and wind stress (Nm^{-2}) anomalies during summer due to the NAO in times when observed coastal SLAs in the MAB and GOM are positive for the 1959–1989 period. (e) Same as (d) but for the 1990–2020 period. (f) Composite differences in SLP and wind stress anomalies due to the NAO between the earlier (1959–1989) and recent (1990–2020) 31 years (e minus d). Panels (g–i) same as (d–f) but for the mean SLP and wind stress anomalies over the two periods and their differences.

positive mean NAO during earlier decades and the negative mean NAO during recent decades (Figure 4c, black dashed lines), suggesting that the decadal change of the NAO toward a negative phase in recent decades reduces SLP near the U.S. northeast coast and increases coastal SLAs via the IB effect. The reduced SLP and northeasterly wind anomalies both act to enhance SLAs north of Cape Hatteras, although the alongshore wind is weak. The SLP pattern due to the NAO during fall also supports a more positive contribution of the IB effect in recent decades compared to earlier decades (Figure S11 in Supporting Information S1).

5. Summary and Discussion

The nonstationary roles of regional forcings from alongshore wind stress and SLP via the IB effect, in driving low-frequency (interannual-to-decadal) sea level variability along the USEC for the 1959–2020 period are investigated in different seasons and regions. Compared to previous studies using annual mean records, we obtain the following new findings:

1. The role of regional forcings in explaining SLA variance along the USEC north of Cape Hatteras increased in recent decades particularly during summer, when the observed sea level variance explained by regional forcings increases by approximately 58% in the MAB and 87% in the GOM from 1959–1989 to 1990–2020 (Figures 2i and 2n). The effects of alongshore wind stress and SLP tend to act destructively in earlier decades, whereas they tend to add constructively in recent decades in relation to large-scale surface climate patterns. No apparent change in the role of regional forcings is detected in the SAB.
2. The increased contribution of the IB effect to coastal SLAs during summer in the MAB and GOM results from changes of SLP during recent decades, when the low SLP anomalies are stronger north of Cape Hatteras (Figure 3).
3. The summertime NAO is largely responsible for the increased role of the IB effect in recent decades (Figure 4).

The regional forcings due to alongshore wind stress and SLP play a large role in driving interannual-decadal USEC SLAs, in agreement with previous studies (e.g., Andres et al., 2013; Piecuch, Dangendorf, et al., 2016; Piecuch, Thompson, & Donohue, 2016; Piecuch & Ponte, 2015; Woodworth et al., 2014). The role of regional forcings, particularly the IB effect, on USEC SLAs north of Cape Hatteras has been enhanced in recent decades during summer seasons. Therefore, the low SLP anomalies during summer in recent decades are an important driver for the increasing risk of coastal highted flooding north of Cape Hatteras. Other forcings such as the remote forcings from the open ocean (e.g., Frederikse et al., 2022; Wang et al., 2022) that are not investigated in this study could also vary with time. For example, the decadal SLAs along the northeastern US coast are enhanced in the second half of the 20th century, which could be related to Labrador Sea heat flux variability (Little, 2022).

This study also finds that the summertime NAO can affect the USEC SLAs by shifting the SLP pattern, while previous studies have demonstrated the importance of NAO on USEC sea level during winter seasons by changing wind stress pattern (Kenigson et al., 2018). The seasonality of the impacts of climate modes, such as the NAO, deserves more attention when using climate mode indices to predict the frequency and intensity of coastal flooding.

Data Availability Statement

The tide-gauge monthly mean sea level is obtained from PSMSL (2021; Holgate et al., 2013), retrieved from http://www.psmsl.org/data/obtaining/. ERA5 monthly atmospheric SLP, wind stress (Hersbach et al., 2019) are provided by the C3S Climate Data Store (https://cds.climate.copernicus.eu/#!/home). The NAO index is downloaded at https://psl.noaa.gov/data/climateindices/list/. The codes of Bayesian DLM are download at https://github.com/mjlaine/dlm.

Acknowledgments
YZ and WH are supported by NOAA Office of Oceanic and Atmospheric Research Climate Program Office (CPO) NA20OAR4310480, and NASA OSTST award 80NSSC21K1190. Part of the work was completed when WH was visiting the International Space Science Institute (ISSI), Bern, Switzerland. She thanks the Johannes Geiss Fellowship from ISSI for providing travel support. MA is supported by NOAA NA20OAR4310480 and thanks to the support of the NOAA/CPO/Climate Variability and Predictability Program.

References

Andres, M., Gawarkiewicz, G. G., & Toole, J. M. (2013). Interannual sea level variability in the western North Atlantic: Regional forcing and remote response. *Geophysical Research Letters*, *40*(22), 5915–5919. https://doi.org/10.1002/2013GL058013

Bell, B., Hersbach, H., Simmons, A., Berrisford, P., Dahlgren, P., Horányi, A., et al. (2021). The ERA5 global reanalysis: Preliminary extension to 1950. *Quarterly Journal of the Royal Meteorological Society*, *147*(741), 4186–4227. https://doi.org/10.1002/qj.4174

Bingham, R. J., & Hughes, C. W. (2009). Signature of the Atlantic meridional overturning circulation in sea level along the east coast of North America. *Geophysical Research Letters*, *36*(2), L02603. https://doi.org/10.1029/2008GL036215

Blaha, J. P. (1984). Fluctuations of monthly sea level as related to the intensity of the Gulf Stream from key west to Norfolk. *Journal of Geophysical Research*, *89*(C5), 8033–8042. https://doi.org/10.1029/JC089iC05p08033

Cazenave, A., & Le Cozannet, G. (2014). Sea level rise and its coastal impacts. *Earth's Future*, *2*, 15–34. https://doi.org/10.1002/2013EF000188

Diabaté, S. T., Swingedouw, D., Hirschi, J. J.-M., Duchez, A., Leadbitter, P. J., Haigh, I. D., & McCarthy, G. D. (2021). Western boundary circulation and coastal sea-level variability in Northern Hemisphere oceans. *Ocean Science*, *17*(5), 1449–1471. https://doi.org/10.5194/os-17-1449-2021

Domingues, R., Goni, G., Baringer, M., & Volkov, D. (2018). What caused the accelerated sea level changes along the U.S. East Coast during 2010–2015? *Geophysical Research Letters*, *45*(24), 13367–13376. https://doi.org/10.1029/2018GL081183

Ezer, T. (2013). Sea level rise, spatially uneven and temporally unsteady: Why the U.S. East Coast, the global tide gauge record, and the global altimeter data show different trends. *Geophysical Research Letters*, *40*(20), 5439–5444. https://doi.org/10.1002/2013GL057952

Ezer, T. (2019). Regional differences in sea level rise between the mid-Atlantic Bight and the South Atlantic Bight: Is the Gulf Stream to blame? *Earth's Future*, *7*, 771–783. https://doi.org/10.1029/2019EF001174

Ezer, T., Atkinson, L. P., Corlett, W. B., & Blanco, J. L. (2013). Gulf Stream's induced sea level rise and variability along the U.S. mid-Atlantic coast. *Journal of Geophysical Research: Oceans*, *118*(2), 685–697. https://doi.org/10.1002/jgrc.20091

Frederikse, T., Lee, T., Wang, O., Kirtman, B., Becker, E., Hamlington, B., et al. (2022). A hybrid dynamical approach for seasonal prediction of sea-level anomalies: A pilot study for Charleston, South Carolina. *Journal of Geophysical Research: Oceans*, *127*(8), e2021JC018137. https://doi.org/10.1029/2021JC018137

Frederikse, T., Simon, K., Katsman, C. A., & Riva, R. (2017). The sea-level budget along the northwest Atlantic coast: GIA, mass changes, and large-scale ocean dynamics. *Journal of Geophysical Research: Oceans*, *122*(7), 5486–5501. https://doi.org/10.1002/2017JC012699

Goddard, P., Yin, J., Griffies, S., & Zhang, S. (2015). An extreme event of sea-level rise along the Northeast coast of North America in 2009–2010. *Nature Communications*, *6*(1), 6346. https://doi.org/10.1038/ncomms7346

Hamlington, B. D., Leben, R. R., Kim, K.-Y., Nerem, R. S., Atkinson, L. P., & Thompson, P. R. (2015). The effect of the El Niño-Southern Oscillation on U.S. regional and coastal sea level. *Journal of Geophysical Research: Oceans*, *120*(6), 3970–3986. https://doi.org/10.1002/2014JC010602

Han, W., Meehl, G. A., Hu, A., Zheng, J., Kenigson, J., Vialard, J., et al. (2017). Decadal variability of the Indian and Pacific walker cells since the 1960s: Do they covary on decadal time scales? *Journal of Climate*, *30*(21), 8447–8468. https://doi.org/10.1175/jcli-d-16-0783.1

Han, W., Stammer, D., Meehl, G. A., Hu, A., Sienz, F., & Zhang, L. (2018). Multi-decadal trend and decadal variability of the regional sea level over the Indian Ocean since the 1960s: Roles of climate modes and external forcing. *Climate*, *6*(2), 51. https://doi.org/10.3390/cli6020051

Han, W., Stammer, D., Thompson, P., Ezer, T., Palanisamy, H., Zhang, X., et al. (2019). Impacts of basin-scale climate modes on coastal sea level: A review. *Surveys in Geophysics*, *40*(6), 1493–1541. https://doi.org/10.1007/s10712-019-09562-8

Hersbach, H., Bell, B., Berrisford, P., Biavati, G., Horányi, A., Muñoz Sabater, J., et al. (2019). ERA5 monthly averaged data on single levels from 1979 to present. *Copernicus Climate Change Service (C3S) Climate Data Store (CDS)*. https://doi.org/10.24381/cds.f17050d7

Holgate, S. J., Matthews, A., Woodworth, P. L., Rickards, L. J., Tamisiea, M. E., Bradshaw, E., et al. (2013). New data systems and products at the permanent service for mean sea level. *Journal of Coastal Research*, *29*(3), 493–504. https://doi.org/10.2112/JCOASTRES-D-12-00175.1

Hong, B. G., Sturges, W., & Clarke, A. J. (2000). Sea level on the U.S. East Coast: Decadal variability caused by open ocean wind-curl forcing. *Journal of Physical Oceanography*, *30*(8), 2088–2098. https://doi.org/10.1175/1520-0485(2000)030<2088:SLOTUS>2.0.CO;2

Hughes, C. W., Fukumori, I., Griffies, S. M., Huthnance, J. M., Minobe, S., Spence, P., et al. (2019). Sea level and the role of coastal trapped waves in mediating the influence of the open ocean on the coast. *Surveys in Geophysics*, *40*(6), 1467–1492. https://doi.org/10.1007/s10712-019-09535-x

Kenigson, J. S., Han, W., Rajagopalan, B., & Jasinski, M. (2018). Decadal shift of NAO-linked interannual sea level variability along the U.S. northeast coast. *Journal of Climate*, *31*(13), 4981–4989. https://doi.org/10.1175/JCLI-D-17-0403.1

Laine, M., Latva-Pukkila, N., & Kyrölä, E. (2014). Analyzing time-varying trends in stratospheric ozone time series using state the space approach. *Atmospheric Chemistry and Physics*, *14*(18), 9707–9725. https://doi.org/10.5194/acp-14-9707-2014

Li, S., Wahl, T., Barroso, A., Coats, S., Dangendorf, S., Piecuch, C., et al. (2022). Contributions of different sea-level processes to high-tide flooding along the U.S. coastline. *Journal of Geophysical Research: Oceans*, *127*(7), e2021JC018276. https://doi.org/10.1029/2021JC018276

Li, Y., Ji, R., Fratantoni, P. S., Chen, C., Hare, J. A., Davis, C. S., & Beardsley, R. C. (2014). Wind-induced interannual variability of sea level slope, along-shelf flow, and surface salinity on the Northwest Atlantic shelf. *Journal of Geophysical Research: Oceans*, *119*(4), 2462–2479. https://doi.org/10.1002/2013JC009385

Little, C. M. (2022). Coastal sea level observations record the twentieth-century enhancement of decadal climate variability. *Journal of Climate*, *36*(1), 243–260. https://doi.org/10.1175/JCLI-D-22-0451.1

Little, C. M., Piecuch, C. G., & Ponte, R. M. (2017). On the relationship between the meridional overturning circulation, alongshore wind stress, and United States East Coast sea level in the Community Earth System Model Large Ensemble. *Journal of Geophysical Research: Oceans*, *122*(6), 4554–4568. https://doi.org/10.1002/2017JC012713

Little, C. M., Piecuch, C. G., & Ponte, R. M. (2021). North American east coast sea level exhibits high power and spatiotemporal complexity on decadal timescales. *Geophysical Research Letters*, *48*(15), e2021GL093675. https://doi.org/10.1029/2021GL093675

Minobe, S., Terada, M., Qiu, B., & Schneider, N. (2017). Western boundary sea level: A theory, rule of thumb, and application to climate models. *Journal of Physical Oceanography*, *47*(5), 957–977. https://doi.org/10.1175/JPO-D-16-0144.1

Neumann, B., Vafeidis, A. T., Zimmermann, J., & Nicholls, R. J. (2015). Future coastal population growth and exposure to sea-level rise and coastal flooding-a global assessment. *PLoS One*, *10*(3), e0118571. https://doi.org/10.1371/journal.pone.0118571

Park, J., & Dusek, G. (2013). ENSO components of the Atlantic multidecadal oscillation and their relation to North Atlantic interannual coastal sea level anomalies. *Ocean Science*, *9*(3), 535–543. https://doi.org/10.5194/os-9-535-2013

Petris, G., Petrone, S., & Campagnoli, P. (2009). Dynamic linear models. In *Dynamic linear models with R* (pp. 31–84). Springer.

Piecuch, C. G., Bittermann, K., Kemp, A. C., Ponte, R. M., Little, C. M., Engelhart, S. E., & Lentz, S. J. (2018). River-discharge effects on United States Atlantic and Gulf coast sea-level changes. *Proceedings of the National Academy of Sciences*, *115*(30), 7729–7734. https://doi.org/10.1073/pnas.1805428115

Piecuch, C. G., Dangendorf, S., Gawarkiewicz, G. G., Little, C. M., Ponte, R. M., & Yang, J. (2019). How is New England coastal sea level related to the Atlantic meridional overturning circulation at 26°N? *Geophysical Research Letters*, *46*(10), 5351–5360. https://doi.org/10.1029/2019GL083073

Piecuch, C. G., Dangendorf, S., Ponte, R. M., & Marcos, M. (2016). Annual sea level changes on the North American northeast coast: Influence of local winds and barotropic motions. *Journal of Climate*, *29*(13), 4801–4816. https://doi.org/10.1175/JCLI-D-16-0048.1

Piecuch, C. G., & Ponte, R. M. (2015). Inverted barometer contributions to recent sea level changes along the northeast coast of North America. *Geophysical Research Letters*, *42*(14), 5918–5925. https://doi.org/10.1002/2015GL064580

Piecuch, C. G., Thompson, P. R., & Donohue, K. A. (2016). Air pressure effects on sea level changes during the twentieth century. *Journal of Geophysical Research: Oceans*, *121*(10), 7917–7930. https://doi.org/10.1002/2016JC012131

Ponte, R. M. (2006). Low-frequency sea level variability and the inverted barometer effect. *Journal of Atmospheric and Oceanic Technology*, *23*(4), 619–629. https://doi.org/10.1175/JTECH1864.1

Ponte, R. M., Carson, M., Cirano, M., Domingues, C. M., Jevrejeva, S., Marcos, M., et al. (2019). Towards comprehensive observing and modeling systems for monitoring and predicting regional to coastal sea level. *Frontiers in Marine Science*, *6*, 437. https://doi.org/10.3389/fmars.2019.00437

Sallenger, A. H., Doran, K. S., & Howd, P. A. (2012). Hotspot of accelerated sea-level rise on the Atlantic coast of North America. *Nature Climate Change*, *2*(12), 884–888. https://doi.org/10.1038/nclimate1597

Sweet, W., Dusek, G., Marcy, D. C., Carbin, G., & Marra, J. (2019). 2018 state of US High tide flooding with a 2019 Outlook.

Sweet, W., Simon, S., Dusek, G., Marcy, D., Brooks, W., Pendleton, M., & Marra, J. (2021). 2021 state of high tide flooding and annual Outlook.

Sweet, W. V., & Zervas, C. (2011). Cool-season sea level anomalies and storm surges along the U.S. East Coast: Climatology and comparison with the 2009/10 El Niño. *Monthly Weather Review*, *139*(7), 2290–2299. https://doi.org/10.1175/MWR-D-10-05043.1

Thompson, P. R., & Mitchum, G. T. (2014). Coherent sea level variability on the North Atlantic western boundary. *Journal of Geophysical Research: Oceans*, *119*(9), 5676–5689. https://doi.org/10.1002/2014JC009999

Valle-Levinson, A., Dutton, A., & Martin, J. B. (2017). Spatial and temporal variability of sea level rise hot spots over the eastern United States. *Geophysical Research Letters*, *44*(15), 7876–7882. https://doi.org/10.1002/2017GL073926

Wang, O., Lee, T., Piecuch, C. G., Fukumori, I., Fenty, I., Frederikse, T., et al. (2022). Local and remote forcing of interannual sea-level variability at Nantucket Island. *Journal of Geophysical Research: Oceans*, *127*(6), e2021JC018275. https://doi.org/10.1029/2021JC018275

Wdowinski, S., Braya, R., Kirtmana, B. P., & Wub, Z. (2016). Increasing flooding hazard in coastal communities due to rising sea level: Case study of Miami Beach, Florida. *Ocean & Coastal Management*, *126*, 1–8. https://doi.org/10.1016/j.ocecoaman.2016.03.002

Woodworth, P. L., Maqueda, M. A. M., Roussenov, M. V., Williams, R. G., & Hughes, C. W. (2014). Mean sea-level variability along the north-east American Atlantic coast and the roles of the wind and the overturning circulation. *Journal of Geophysical Research: Oceans*, *119*(12), 8916–8935. https://doi.org/10.1002/2014JC010520

Woodworth, P. L., Melet, A., Marcos, M., Ray, R. D., Wöppelmann, G., Sasaki, Y. N., et al. (2019). Forcing factors affecting sea level changes at the coast. *Surveys in Geophysics*, *40*(6), 1351–1397. https://doi.org/10.1007/s10712-019-09531-1

Yin, J., & Goddard, P. B. (2013). Oceanic control of sea level rise patterns along the East Coast of the United States. *Geophysical Research Letters*, *40*(20), 5514–5520. https://doi.org/10.1002/2013GL057992

References From the Supporting Information

Barnston, A. G., & Livezey, R. E. (1987). Classification, seasonality and persistence of low-frequency atmospheric circulation patterns. *Monthly Weather Review*, *115*(6), 1083–1126. https://doi.org/10.1175/1520-0493(1987)115<1083:CSAPOL>2.0.CO;2

Li, J., & Clarke, A. J. (2005). Interannual flow along the northern coast of the Gulf of Mexico. *Journal of Geophysical Research*, *110*(C11), C11002. https://doi.org/10.1029/2004JC002606

Ponte, R. M. (1992). The sea level response of a stratified ocean to barometric pressure forcing. *Journal of Physical Oceanography*, *22*(1), 109–113. https://doi.org/10.1175/1520-0485(1992)022<0109:TSLROA>2.0.CO;2

Wunsch, C., & Stammer, D. (1997). Atmospheric loading and the oceanic "inverted barometer" effect. *Reviews of Geophysics*, *35*(1), 79–107. https://doi.org/10.1029/96RG03037